Globally Optimal Hand-Eye Calibration

Thomas Ruland
Ulm University
Ulm, Germany
thomas.ruland@uni-ulm.de

Tomas Pajdla
Czech Technical University
Prague, Czech Republic
pajdla@cmp.felk.cvut.cz

Lars Krüger
Daimler AG
Ulm, Germany
lars.krueger@daimler.com

Abstract

This paper introduces simultaneous globally optimal hand-eye self-calibration in both its rotational and translational components. The main contributions are new feasibility tests to integrate the hand-eye calibration problem into a branch-and-bound parameter space search. The presented method constitutes the first guaranteed globally optimal estimator for simultaneous optimization of both components with respect to a cost function based on reprojection errors. The system is evaluated in both synthetic and real world scenarios. The employed benchmark dataset is published online[1] *to create a common point of reference for evaluation of hand-eye self-calibration algorithms.*

1. Introduction

Fig. 3a shows a common application scenario for hand-eye calibration, where a camera is mounted to a robot's end-effector. The objective is to determine the Euclidean transformation between the camera and the end-effector, which is required to relate perceived objects in both coordinate systems. The motion of the end-effector is known accurately from the robot's forward kinematics. The camera motion traditionally is determined using known calibration objects in the scene. The first approaches to solve the hand-eye calibration problem recovered rotational and translational parameters sequentially [10, 14]. Horaud and Dornika [8] as well as Daniilidis [3] presented combined approaches to solve for both components simultaneously. Starting in assembly robotics, hand-eye calibration has spread into a multitude of usage scenarios including mobile [4] and medical robotics [12]. In many of these scenarios, traditional hand-eye calibration based on observation of known calibration targets is not applicable. Instead structure from motion algorithms are applied to determine the camera motion[1, 12].

Very recently, globally optimal solutions to common structure and motion problems in computer vision were introduced. The framework presented by Kahl and Hartley in [9] allows to compute the globally optimal solution to problems like triangulation, camera resectioning, and homography estimation. In [5], they added a branch-and-bound search over the rotation space to this framework. On the basis of this framework, Seo et al. [13] were able to propose a new approach for solving the hand-eye orientation problem. Their algorithm recovers the rotational component of the hand-eye transformation globally optimal but requires all translations in the system to be zero. Heller et al. [7] proposed an optimal algorithm for recovery of hand-eye translation while requiring known rotation.

This paper introduces simultaneous globally optimal hand-eye self-calibration in both its rotational and translational components, while only requiring a rough upper bound of the hand-eye translation's length. To the authors' knowledge, no optimal solution with respect to a geometrically meaningful objective function based on reprojection errors has yet been presented to the full hand-eye calibration problem. The main contribution are new feasibility tests to integrate the hand-eye calibration problem into a branch-and-bound parameter space search.

2. Problem Formulation

The objective of hand-eye calibration is to determine the Euclidean transformation $\mathtt{X}$ between a robot's end-effector and camera coordinate frame. Hand-eye calibration builds upon the fact that hand and eye are rigidly coupled. The robot executes N hand motions and measures them using forward kinematics as the transformation $\mathtt{B}^k$, $k \in \{1, N\}$. The motion is observed by the camera as a transformation $\mathtt{A}^k$ in its own coordinate frame (Fig. 1). Both motions are coupled by the common hand-eye calibration equation

$$\mathtt{A}^k = \mathtt{X}\,\mathtt{B}^k\,\mathtt{X}^{-1} \in \mathrm{SE}\,(3)\,. \tag{1}$$

It can be decomposed in its rotational and translational parts

$$\mathtt{R}_A^k = \mathtt{R}_X\,\mathtt{R}_B^k\,\mathtt{R}_X^{-1} \in \mathrm{SO}\,(3) \tag{2}$$

$$\mathbf{t}_A^k = \mathtt{R}_X\,\mathbf{t}_B^k + \mathtt{R}_X\left({\mathtt{R}_B^k}^{-1} - \mathtt{I}\right)\mathbf{t}_X \in \mathbb{R}^3. \tag{3}$$

[1] See http://hand-eye-calibration.com or contact the first author

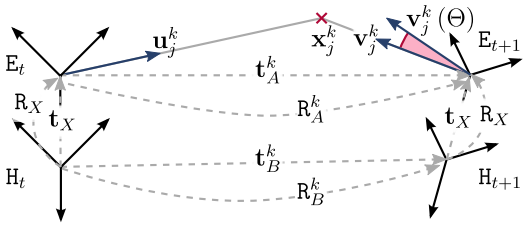

Figure 1: Exemplary hand-eye geometry with the coordinate frames of the eye $\mathtt{E}$ and the hand $\mathtt{H}$ at two subsequent points in time. Eye and hand motions are denoted by a subscript A and B respectively. The two hand-eye transformations are marked by a subscript X. The scene point $\mathbf{x}_j^k$ is observed by the two cameras in the directions $\mathbf{u}_j^k$ and $\mathbf{v}_j^k$.

In contrast to the majority of previous contributions on hand-eye calibration, the camera motion $\mathtt{A}^k$ is not explicitly estimated in this work. Instead, the task is interpreted as an instance of the relative pose problem. This way the camera motion, which is intrinsically encoded in the motion of image features, is used directly.

To improve readability, a superscript k is used in this work to indicate the motion index. In no case it represents the k-th power of the respective variable.

2.1. Objective Function

The objective function, which is globally minimized in this work, is based on the relative pose problem. Its goal is to find the relative Euclidean transformation $\mathtt{A}^k$ between two cameras with identical calibration matrices $\mathtt{K}$, given a set of image correspondences $\mathbf{p}_j^k \leftrightarrow \mathbf{q}_j^k \; j = 1, \ldots, M\,(k)$. They are observations of unknown 3D points $\mathbf{x}_j^k$ and their projection is modeled by $\mathbf{p}_j^k(\Theta) \cong \mathtt{K}\,\mathbf{x}_j^k$ and $\mathbf{q}_j^k(\Theta) \cong \mathtt{K}\,\mathtt{A}^k\,\mathbf{x}_j^k$ for all j, where Θ collects all model parameters and thus describes $\mathtt{A}^k$ and $\mathbf{x}_j^k$. Usually, both the transformation $\mathtt{A}^k$ as well as the scene points $\mathbf{x}_j^k$ are recovered during relative pose estimation.

In presence of noise, there is no exact solution to the relative pose problem. In this case it is generally considered optimal to minimize the reprojection error between the points $\mathbf{p}_j^k, \mathbf{q}_j^k$ measured by the camera and points $\mathbf{p}_j^k(\Theta), \mathbf{q}_j^k(\Theta)$ generated by the discussed projection model. The reprojection error is given by the distances $\|\mathbf{p}_j^k - \mathbf{p}_j^k(\Theta)\|$ and $\|\mathbf{q}_j^k - \mathbf{q}_j^k(\Theta)\|$. The cameras are assumed to be intrinsically calibrated in this work. For small reprojection errors it is thus equivalent to minimize the angular error between the incoming rays of $\mathbf{p}_j^k$ and $\mathbf{q}_j^k$. Fig. 1 illustrates how both rays originate in the respective camera center. Their direction towards the scene point $\mathbf{x}_j^k$ is encoded by unit directional vectors $\mathbf{u}_j^k \cong \mathtt{K}^{-1}\,\mathbf{p}_j^k$ and $\mathbf{v}_j^k \cong \mathtt{K}^{-1}\,\mathbf{q}_j^k$. Image measurements in this work are thus represented as points on the image sphere and the reprojection error is given by the angles

$$\angle\left(\mathbf{u}_j^k, \mathbf{u}_j^k(\Theta)\right) \quad \text{and} \quad \angle\left(\mathbf{v}_j^k, \mathbf{v}_j^k(\Theta)\right) \tag{4}$$

between the measured directions $\mathbf{u}_j^k, \mathbf{v}_j^k$ and the modelled directions $\mathbf{u}_j^k(\Theta), \mathbf{v}_j^k(\Theta)$. The directional representation of image measurements allows the formulation of the relative pose problem as the angle between the measured and the modelled object directions. The transformation $\mathtt{A}^k$ decomposes into the rotation $\mathtt{R}_A^k \in \mathrm{SO}(3)$ and the translation $\mathbf{t}_A^k \in \mathbb{R}^3$. The goal is to optimize

$$\angle\left(\mathbf{u}_j^k, \mathbf{x}_j^k\right) \longrightarrow \min \tag{5}$$

$$\angle\left(\mathbf{v}_j^k, \mathtt{R}_A^k\left(\mathbf{x}_j^k - \mathbf{t}_A^k\right)\right) \longrightarrow \min. \tag{6}$$

Fig. 1 again illustrates this formulation. The scalar angular differences for all scene points can be combined into a single vector. L_∞-approaches optimize the L_∞-norm (maximum component) of this difference vector. The goal is to globally minimize the objective function or the *cost* over all possible rotations and translations. This optimization problem is commonly given in the minimax form.

$$\min_{\mathtt{R}_A^k, \mathbf{t}_A^k, \mathbf{x}_j^k} \max_{k,j} \begin{cases} \angle\left(\mathbf{u}_j^k, \mathbf{x}_j^k\right) \\ \angle\left(\mathbf{v}_j^k, \mathtt{R}_A^k\left(\mathbf{x}_j^k - \mathbf{t}_A^k\right)\right) \end{cases} \tag{7}$$

Substituting $\mathtt{R}_\mathtt{A}^\mathtt{k}$ by $\mathtt{R}_X\,\mathtt{R}_B^k\,\mathtt{R}_X^{-1}$ using (2) allows to estimate the hand-eye rotation $\mathtt{R}_X$ and results in the final optimization problem:

$$\min_{\mathtt{R}_X, \mathbf{t}_A^k, \mathbf{x}_j^k} \max_{k,j} \begin{cases} \angle\left(\mathbf{u}_j^k, \mathbf{x}_j^k\right) \\ \angle\left(\mathbf{v}_j^k, \mathtt{R}_X\mathtt{R}_B^k\mathtt{R}_X^{-1}\left(\mathbf{x}_j^k - \mathbf{t}_A^k\right)\right) \end{cases} \tag{8}$$

Its objective function is non-convex and generally paved with local minima. This property prohibits a global optimization using gradient descent methods. Notice that the camera translation $\mathbf{t}_A^k$ is not yet substituted by its hand-eye equivalent in (3). The estimation of the hand-eye translation $\mathbf{t}_X$ is postponed to Section 3.2.

3. Algorithm

3.1. Branch-and-Bound Search

The hand-eye rotation $\mathtt{R}_X$ is represented by its angle $\gamma \in \mathbb{R}$ and axis $\mathbf{r} \in \mathbb{R}^3$ with $\|\mathbf{r}\| = 1$. Both are encoded in the parameter vector $\xi = \gamma\,\mathbf{r}$. All rotations are represented by the vectors in the closed ball of radius π. The algorithm's initial search range is the enclosing cube with half side length π. The branch-and-bound search divides the parameter space into cubes of half side length σ. The key principle is that it is not necessary to solve the optimization problem on each cube exactly. Instead only a lower bound for the optimal solution within a cube is required. This bound has to converge towards the optimal solution as the size of the cube decreases.

During search, the algorithm keeps track of the currently best parameter vector $\Theta^\star$ with its cost $\epsilon_{\min}$. The algorithm holds a queue Q of cubes, which is empty in the beginning. The individual steps are:

1. **Initialization:** Set $\Theta^\star$ arbitrarily and update $\epsilon_{\min}$. Add the initial cube, which contains the whole parameter space, to the queue Q.
2. **Feasibility Test:** Test each cube in the queue if it may contain a solution, which provides a cost improvement with respect to $\epsilon_{\min}$. If no such solution exists the cube can be discarded safely.
3. Otherwise:
   (a) **Obj. Function Evaluation:** Evaluate objective function on an arbitrary parameter vector inside the cube. Update $\Theta^\star$ and $\epsilon_{\min}$ if the associated cost is smaller.
   (b) **Recursion:** Subdivide the cube into eight subcubes with half side length, append them to the queue Q and start over from 2.

The feasibility test, which is formulated in greater detail in Problem 1, has to evaluate an infinite number of parameters. To reduce computational complexity, the basic idea is to find sufficient criteria for the infeasibility of a parameter space cube, which can be evaluated very efficiently. In the limit case of zero cube volume, these criteria also have to become necessary conditions for cube infeasibility to ensure convergence of the algorithm. In the following, a chain of feasibility problems is developed. Their satisfaction is implied by the original Problem 1.

$$\text{Problem 1} \rightarrow \text{Problem 2} \rightarrow \text{Problem 3} \tag{9}$$

The contraposition yields a sufficient condition for the infeasiblity of a parameter cube in the sense of Problem 1.

$$\neg\ \text{Problem 1} \leftarrow \neg\ \text{Problem 2} \leftarrow \neg\ \text{Problem 3} \tag{10}$$

During rotation space search, the algorithm efficiently detects cubes which are infeasible in the sense of Problem 3, implies infeasibility of Problem 1 and safely discards them. In the following, Problems 1-3 are introduced successively. Lemma 5 then proves the implication chain.

3.2. Feasibility Test

The question to be answered in the feasibility test is whether there might be a solution inside a cube of parameters, which provides a cost reduction with respect to the current minimum. This section introduces a feasibility test for the hand-eye calibration problem. Problem 1 formulates this question of a possible cost improvement for the optimization problem (8). A cube is given by the restricted domain D. The L_∞-norm over the difference vector is replaced by constraints onto every correspondence $\mathbf{u}_{j,k} \leftrightarrow \mathbf{v}_{j,k}$. The current cost minimum is denoted by $\epsilon_{\min}$.

Problem 1 *Standard feasibility problem for orientation search*

Given	D, $\epsilon_{\min}$
do exist	$\mathbf{t}_A^k$, $\mathbf{x}_j^k$, $\mathtt{R}_X \in D$
such that	$\angle\left(\mathbf{u}_j^k, \mathbf{x}_j^k\right) \leq \epsilon_{\min}$
and	$\angle\left(\mathbf{v}_j^k, \mathtt{R}_X\, \mathtt{R}_B^k\, \mathtt{R}_X^{-1}\left(\mathbf{x}_j^k - \mathbf{t}_A^k\right)\right) \leq \epsilon_{\min}$
for	$j = 1, \ldots, N\,(k)$, $k = 1, \ldots, M$

It is quite complex to give an answer to this problem directly since even the restricted domain inside the cube still contains an infinite number of possible parameters. Instead of evaluating all these parameters, Problem 2 fixes the rotation $\mathtt{R}_X$ to the parameter at the center of the cube $\bar{\mathtt{R}}_X$. Then it infers a lower bound for the minimum cost over all parameters inside the cube. This is possible by introducing a bound on the maximum objective function improvements for similar parameter vectors inside a small restricted region. The result is a relaxed problem based on the parameters at the center of the cube.

Problem 2 *Relaxed feasibility problem for orientation search*

Given	$\bar{\mathtt{R}}_X$ corresponding to center of D, σ, $\epsilon_{\min}$
do exist	$\mathbf{t}_A^k$, $\mathbf{x}_j^k$
such that	$\angle\left(\mathbf{u}_j^k, \mathbf{x}_j^k\right) \leq \epsilon_{\min}$
and	$\angle\left(\mathbf{v}_j^k, \bar{\mathtt{R}}_X\, \mathtt{R}_B^k\, \bar{\mathtt{R}}_X^{-1}\left(\mathbf{x}_j^k - \mathbf{t}_A^k\right)\right)$
	$\leq \epsilon_{\min} + 2\,\varphi_{\max} \sin\left(\sigma\sqrt{3}/2\right)$
for	$j = 1, \ldots, N\,(k)$, $k = 1, \ldots, M$

Lemma 1 (Relation of Problem 1 and 2)**.** *If there exists a feasible solution to Problem 1, then there is also a feasible solution to Problem 2.*

The following proof of Lemma 1 is based on the work of Seo et al. [13] and also applies lemmas from the contribution of Hartley and Kahl [5]. Due to space constraints, the lemmas used could not be restated in this paper.

Proof. Let $\left(\tilde{\mathtt{R}}_X, \tilde{\mathbf{t}}_A^k, \tilde{\mathbf{x}}_j^k\right)$ be a feasible solution to Problem 1 in the restricted domain D. The proof shows, that $\left(\tilde{\mathbf{t}}_A^k, \tilde{\mathbf{x}}_j^k\right)$ is a feasible solution to Problem 2 for the rotation $\bar{\mathtt{R}}_X$ corresponding to the center of D. Denote $\tilde{\mathbf{s}}_j^k = \tilde{\mathbf{x}}_j^k - \tilde{\mathbf{t}}_A^k$ and the half side length of the cube D by σ. The angle axis representation of the hand rotation $\mathtt{R}_B^k$ is β^k. The first constraint $\angle\left(\mathbf{u}_j^k, \mathbf{x}_j^k\right) \leq \epsilon_{\min}$ of Problem 2 is satisfied for all correspondences since it is equal in both problems. The second constraint, which is formulated for every correspondence individually, is replaced by a single condition on the maximum error over all correspondences. The following inequalities derive a lower bound on the optimal objective function value inside a cube with rotation $\bar{\mathtt{R}}_X$ represented at

the cube's center.

$$\begin{aligned}
&\max_{j,k} \angle\left(\mathbf{v}_j, \bar{\mathtt{R}}_X \mathtt{R}_B^k \bar{\mathtt{R}}_X^{-1}\left(\tilde{\mathbf{x}}_j^k - \tilde{\mathbf{t}}_A^k\right)\right) \\
&\leq \max_{j,k} \angle\left(\mathbf{v}_j, \tilde{\mathtt{R}}_X \mathtt{R}_B^k \tilde{\mathtt{R}}_X^{-1}\left(\tilde{\mathbf{x}}_j^k - \tilde{\mathbf{t}}_A^k\right)\right) \qquad (11)\\
&\quad + \max_{j,k} \angle\left(\tilde{\mathtt{R}}_X \mathtt{R}_B^k \tilde{\mathtt{R}}_X^{-1} \tilde{\mathbf{s}}_j^k, \bar{\mathtt{R}}_X \mathtt{R}_B^k \bar{\mathtt{R}}_X^{-1} \tilde{\mathbf{s}}_j^k\right) \\
&\leq \epsilon_{\min} + \max_{k} \angle\left(\tilde{\mathtt{R}}_X \mathtt{R}_B^k \tilde{\mathtt{R}}_X^{-1}, \bar{\mathtt{R}}_X \mathtt{R}_B^k \bar{\mathtt{R}}_X^{-1}\right) \qquad (12)\\
&\leq \epsilon_{\min} + \max_{k} \left\| \tilde{\mathtt{X}}\, \beta^k - \bar{\mathtt{X}}\, \beta^k \right\| \qquad (13)\\
&= \epsilon_{\min} + \max_{k} \left\| \beta^k - \tilde{\mathtt{X}}^{-1}\, \bar{\mathtt{X}}\, \beta^k \right\| \qquad (14)\\
&\leq \epsilon_{\min} + \max_{k} 2 \left\| \beta^k \right\| \sin\left(\sigma\sqrt{3}/2\right) \qquad (15)\\
&= \epsilon_{\min} + 2\, \varphi_{\max} \sin\left(\sigma\sqrt{3}/2\right), \qquad (16)
\end{aligned}$$

The maximum rotation angle over all hand motions is given by $\varphi_{\max}$. Notice the usage of the triangle inequality in (11), Lemma 1 of [5] in (12), Lemma 1 and 4 of [13] in (13) and Lemma 2 of [13] in (15). The Lemmas could not be included due to space constraints. In (12) the objective function value for the rotation $\tilde{\mathtt{R}}_X$ can be bounded from above by $\epsilon_{\min}$ since $\tilde{\mathtt{R}}_X$ is a feasible solution to Problem 1.

Since the second constraint is satisfied for the maximum angular error over all correspondences, it is also satisfied for every individual correspondence. The parameter set $\left(\tilde{\mathbf{t}}_A^k, \tilde{\mathbf{x}}_j\right)$ is a feasible solution to Problem 2 for rotation $\bar{\mathtt{R}}_X$ corresponding to the center of D. □

The angular constraints in Problem 2 induce two circular cones with axes $\mathbf{u}_j^k$ and $\mathbf{v}_j^k$ for each correspondence. Problem 2 asks for the existence of a point $\mathbf{x}_j^k$ within both cones, thus it practically asks whether the two cones intersect. A necessary condition for this intersection is the coplanarity of both cones and the translation vector $\mathbf{t}_A^k$ between the camera centers. More precisely, there has to exist a ray within the first cone, which is coplanar with a ray within the second cone and the translation $\mathbf{t}_A^k$. In the derivation of their "Linear Programming Solution for Relative Pose" Hartley and Kahl [5] show how the cone coplanarity condition induces linear constraints on $\mathbf{t}_A^k$. In their work, these linear constraints are illustrated as planes, which are tangent to both cones. The wedge in-between both planes contains the feasible $\mathbf{t}_A^k$, which satisfy the coplanarity condition. The two constraint planes can be expressed as

$$\begin{aligned}
{\mathbf{n}_j^k}^{\mathsf{T}}\, \mathbf{t}_A^k &\geq 0 \qquad (17)\\
{\mathbf{m}_j^k}^{\mathsf{T}}\, \mathbf{t}_A^k &\geq 0,
\end{aligned}$$

where $\mathbf{n}_j^k$ and $\mathbf{m}_j^k \in \mathbb{R}^3$ with $\left\|\mathbf{n}_j^k\right\| = \left\|\mathbf{m}_j^k\right\| = 1$. They represent the two plane normals for every correspondence j of every motion k. Their exact derivation from the parameters in Problem 2 is given in [5].

In Problem 2, only the rotational component of the hand motion is matched with the feature movements. Since hand and eye are rigidly coupled, the translational component has to be constrained too. Following from (3), the camera translation $\mathbf{t}_A^k$ is an affine function of $\mathbf{t}_X$. Substituting it in (17) yields two new constraints on the hand-eye translation $\mathbf{t}_X$.

$$\begin{aligned}
{\mathbf{n}_j^k}^{\mathsf{T}} \left(\tilde{\mathtt{R}}_X\, {\mathtt{R}_B^k}^{-1} - \tilde{\mathtt{R}}_X\right) \mathbf{t}_X + {\mathbf{n}_j^k}^{\mathsf{T}}\, \tilde{\mathtt{R}}_X\, \mathbf{t}_B^k \geq 0 \qquad (18)\\
{\mathbf{m}_j^k}^{\mathsf{T}} \left(\tilde{\mathtt{R}}_X\, {\mathtt{R}_B^k}^{-1} - \tilde{\mathtt{R}}_X\right) \mathbf{t}_X + {\mathbf{m}_j^k}^{\mathsf{T}}\, \tilde{\mathtt{R}}_X\, \mathbf{t}_B^k \geq 0
\end{aligned}$$

They constitute the *cone coplanarity constraint on the hand-eye translation* $\mathbf{t}_X$. Those $\mathbf{t}_X$, which satisfy both constraints, produce camera translations $\mathbf{t}_A^k$ which are coplanar with each pair of cones for every correspondence. The left side of inequalities (18) will be named the *coplanarity condition values* in the following.

The exact hand-eye rotation $\tilde{\mathtt{R}}_X$, which yields the cost improvement in Problem 2, is unknown and thus (18) cannot be evaluated directly. The new feasibility Problem 3 is introduced in the following. It fixes the rotation to $\bar{\mathtt{R}}_X$, which is represented by the parameter at the center of the cube. To fix the rotation to the cube center, an upper bound for the maximum coplanarity condition value over all parameter inside the cube is introduced. This upper bound is then tested against the condition ≥ 0. The result is the relaxed Problem 3 based only on the parameter vector at the center of the cube. A subsequent lemma then shows that every solution $\tilde{\mathbf{t}}_X$ to the exact coplanarity condition based on $\tilde{\mathtt{R}}_X$ causes also the upper bound based only on $\bar{\mathtt{R}}_X$ to satisfy the ≥ 0 condition. For the derivation of Problem 3, the following two lemmas are required.

Lemma 2 introduces an upper bound for the projection's value $\mathbf{n}^{\mathsf{T}}\mathtt{R}\mathbf{v}$ of a rotated vector $\mathtt{R}\mathbf{v}$ onto a normalized vector $\mathbf{n}$ over a restricted domain of rotations.

Lemma 2 (Upper bound of projection value)**.** *For all* $\mathbf{v}, \mathbf{n} \in \mathbb{R}^3$ *with* $\|\mathbf{n}\| = 1$, $\alpha = \angle(\mathbf{n}, \mathtt{R}'\mathbf{v})$, $\angle(\mathtt{R}\mathbf{v}, \mathtt{R}'\mathbf{v}) \leq \gamma$ *and* $\mathtt{R}, \mathtt{R}' \in \mathrm{SO}(3)$ *holds:*

$$\mathbf{n}^{\mathsf{T}}\mathtt{R}\mathbf{v} \leq \mathbf{n}^{\mathsf{T}}\mathtt{R}'\mathbf{v} + \|\mathbf{v}\| \begin{cases} 1 - \cos(\alpha) & \text{if } \alpha < \gamma, \\ \cos(\alpha - \gamma) - \cos(\alpha) & \text{otherwise.} \end{cases}$$

Proof. The scalar product $\mathbf{n}^{\mathsf{T}}\mathtt{R}\mathbf{v}$ may be interpreted as the projection of $\mathtt{R}\mathbf{v}$ onto $\mathbf{n}$. All possible $\mathtt{R}\mathbf{v}$ with $\angle(\mathtt{R}\mathbf{v}, \mathtt{R}'\mathbf{v}) \leq \gamma$ span a circular cone in 3D with principal axis $\mathtt{R}'\mathbf{v}$. There are two possible configurations. Either $\mathbf{n}$ is located in this cone or not. **Case n within cone ($\alpha < \gamma$):** The maximum value for the projection $\mathbf{n}^{\mathsf{T}}\mathtt{R}\mathbf{v}$ occurs for $\mathbf{n}$ and $\mathtt{R}\mathbf{v}$ being parallel. Since $\|n\| = 1$ and $\mathtt{R}$ being an isometry, the value of the projection is $\|v\|$. The maximum increase is thus given by $\delta = \|v\| - \mathbf{n}^{\mathsf{T}}\mathtt{R}'\mathbf{v} = \|v\|(1 - \cos(\alpha))$. **Case n not within cone ($\alpha \geq \gamma$):** The maximum projection value is achieved for the $\mathtt{R}\mathbf{v}$

with the smallest $\angle(\mathbf{n}, \mathtt{R}\mathbf{v})$. The smallest achievable angle is $\alpha - \gamma$. Thus the largest possible projection value is $\max_{\mathtt{R}} \mathbf{n}^\mathsf{T}\mathtt{R}\mathbf{v} = \|v\| \cos(\alpha - \gamma)$ and the maximum increase $\delta = \|v\| (\cos(\alpha - \gamma) - \cos(\alpha))$. □

Lemma 3 generalizes the upper bound to an unknown vector $\mathbf{v} \in \mathbb{R}^3$ satisfying $\|\mathbf{v}\| \leq L_v$.

Lemma 3 (Upper bound of projection value for unknown vector $\mathbf{v}$)**.** *For all $\mathbf{v}, \mathbf{n} \in \mathbb{R}^3$ with $\|\mathbf{n}\| = 1$, $\angle(\mathtt{R}\mathbf{v}, \mathtt{R}'\mathbf{v}) \leq \gamma$, $\mathtt{R}, \mathtt{R}' \in \mathrm{SO}(3)$ and known upper bound of $\mathbf{v}$'s Euclidean norm $L_v \geq \|v\|$ holds:*

$$\mathbf{n}^\mathsf{T}\mathtt{R}\mathbf{v} \leq \mathbf{n}^\mathsf{T}\mathtt{R}'\mathbf{v} + 2\, L_v \cos\left(\frac{\pi - \gamma}{2}\right). \tag{19}$$

Proof. The value of the projection increase is maximized over all possible angles $\alpha = \angle(\mathbf{n}, \mathtt{R}'\mathbf{v})$. **Case $\alpha < \gamma$:** Since $0 \leq \gamma \leq \pi$ there holds $0 \leq \alpha < \gamma \leq \pi$. The maximum projection increase from Lemma 2 is $\delta(\alpha) = L_v(1 - \cos(\alpha))$. Its first derivative vanishes only once in $\alpha \in [0, \pi)$ at $\alpha = 0$, where its second derivative reveals that $\delta(0)$ is a local minimum. The maximum values are thus reached for α's only remaining limit case $\alpha \to \gamma$. Thus the maximum increase of projection value is $L_v(1 - \cos(\gamma))$. **Case $\alpha \geq \gamma$:** In this case it holds $0 \leq \gamma \leq \alpha \leq \pi$. The first derivative of $\delta(\alpha) = L_v(\cos(\alpha - \gamma) - \cos(\alpha))$ vanishes for $\alpha = \frac{\pi+\gamma}{2}$, where its second derivative is nonpositive. The maximum increase of the projection value is thus $2L_v \cos\left(\frac{\pi-\gamma}{2}\right)$. Since $2\cos(\left(\frac{\pi-\gamma}{2}\right) \geq 1 - \cos(\gamma)$ for $\gamma \in [0, \pi]$, the maximum increase of the projection value over all α is given by $2L_v \cos\left(\frac{\pi-\gamma}{2}\right)$. □

The following problem introduces the relaxed coplanarity condition for hand-eye translation $\mathbf{t}_X$ based only on the rotation $\bar{\mathtt{R}}_X$ represented by the center of a prameter cube.

Problem 3 *Cone coplanarity constraint on $\mathbf{t}_X$*

Given $\bar{\mathtt{R}}_X$ corresponding to center of D, $\sigma, \mathbf{n}_j^k, \mathbf{m}_j^k$

do exist $\mathbf{t}_X$

such that
$$\begin{aligned}&\mathbf{n}_j^{k\mathsf{T}} \left(\bar{\mathtt{R}}_X\, \mathtt{R}_B^{k\,-1} - \bar{\mathtt{R}}_X\right) \mathbf{t}_X + \mathbf{n}_j^{k\mathsf{T}}\, \bar{\mathtt{R}}_X\, \mathbf{t}_B^k \\ &\quad + 4L_X \cos\left(\left(\pi - \sqrt{3}\sigma\right)/2\right) \\ &\quad + \left\|\mathbf{t}_B^k\right\| \left(1 - \cos\left(\angle\left(\mathbf{n}_j^k, \bar{\mathtt{R}}_X \mathbf{t}_B^k\right)\right)\right) \\ &\quad \geq 0\end{aligned}$$

and
$$\begin{aligned}&\mathbf{m}_j^{k\mathsf{T}} \left(\bar{\mathtt{R}}_X\, \mathtt{R}_B^{k\,-1} - \bar{\mathtt{R}}_X\right) \mathbf{t}_X + \mathbf{m}_j^{k\mathsf{T}}\, \bar{\mathtt{R}}_X\, \mathbf{t}_B^k \\ &\quad + 4L_X \cos\left(\left(\pi - \sqrt{3}\sigma\right)/2\right) \\ &\quad + \left\|\mathbf{t}_B^k\right\| \left(1 - \cos\left(\angle\left(\mathbf{m}_j^k, \bar{\mathtt{R}}_X \mathbf{t}_B^k\right)\right)\right) \\ &\quad \geq 0\end{aligned}$$

for $j = 1, \ldots, N(k), k = 1, \ldots, M$

Lemma 4 (Relation of Problem 3 and inequalities (18))**.** *A solution $\tilde{\mathbf{t}}_X$ to* (18) *with $\left\|\tilde{\mathbf{t}}_X\right\| \leq L_X$ is a feasible solution in Problem 3.*

Proof. Let $\tilde{\mathbf{t}}_X$ be a solution to the inequalities (18) with $\left\|\tilde{\mathbf{t}}_X\right\| \leq L_X$. The proof will show the following two inequalities.

$$\begin{aligned}0 &\leq \mathbf{n}_j^{k\mathsf{T}} \left(\tilde{\mathtt{R}}_X\, \mathtt{R}_B^{k\,-1} - \tilde{\mathtt{R}}_X\right) \mathbf{t}_X + \mathbf{n}_j^{k\mathsf{T}}\, \tilde{\mathtt{R}}_X\, \mathbf{t}_B^k && (20)\\ &\leq \mathbf{n}_j^{k\mathsf{T}} \left(\bar{\mathtt{R}}_X\, \mathtt{R}_B^{k\,-1} - \bar{\mathtt{R}}_X\right) \mathbf{t}_X + \mathbf{n}_j^{k\mathsf{T}}\, \bar{\mathtt{R}}_X\, \mathbf{t}_B^k + \delta && (21)\end{aligned}$$

The first inequality is satisfied by choice of $\tilde{\mathbf{t}}_X$. For the second inequality to be true, its three additive components have to satisfy the following inequalities

$$\begin{aligned}\mathbf{n}_j^{k\mathsf{T}} \tilde{\mathtt{R}}_X \mathtt{R}_B^k \tilde{\mathbf{t}}_X &\leq \mathbf{n}_j^{k\mathsf{T}} \bar{\mathtt{R}}_X \mathtt{R}_B^k \tilde{\mathbf{t}}_X + \delta_1 && (22)\\ -\mathbf{n}_j^{k\mathsf{T}} \tilde{\mathtt{R}}_X \tilde{\mathbf{t}}_X &\leq -\mathbf{n}_j^{k\mathsf{T}} \bar{\mathtt{R}}_X \tilde{\mathbf{t}}_X + \delta_2 && (23)\\ \mathbf{n}_j^{k\mathsf{T}} \tilde{\mathtt{R}}_X \mathbf{t}_B^k &\leq \mathbf{n}_j^{k\mathsf{T}} \bar{\mathtt{R}}_X \mathbf{t}_B^k + \delta_3, && (24)\end{aligned}$$

where $\delta = \delta_1 + \delta_2 + \delta_3$. Using Lemma 1 and 4 of [5] it holds:

$$\angle\left(\tilde{\mathtt{R}}_X \mathbf{v}, \bar{\mathtt{R}}_X \mathbf{v}\right) \leq \mathrm{d}_\angle\left(\tilde{\mathtt{R}}_X, \bar{\mathtt{R}}_X\right) \leq \sqrt{3}\sigma \quad \forall \mathbf{v} \in \mathbb{R}^3, \tag{25}$$

where $\sqrt{3}\sigma$ is the maximum Euclidean distance in the parameter space between the cube center (representing $\bar{\mathtt{R}}_X$) and any other parameter within the cube (representing $\tilde{\mathtt{R}}_X$). The first two inequalities (22) and (23) are satisfied for $\delta_{1,2} = 2L_X \cos\left(\left(\pi - \sqrt{3}\sigma\right)/2\right)$ following Lemma 3 with $\gamma = \sqrt{3}\sigma$. The third inequality (24) follows from Lemma 2 for

$$\delta_3 = \left\|\mathbf{t}_B^k\right\| \begin{cases} 1 - \cos(\alpha) & \text{if } \alpha < \gamma, \\ \cos(\alpha - \gamma) - \cos(\alpha) & \text{otherwise.} \end{cases} \tag{26}$$

and $\alpha = \angle\left(\mathbf{n}_j^k, \bar{\mathtt{R}}_X \mathbf{t}_B^k\right)$. Thus inequality (21) holds for $\tilde{\mathbf{t}}_X$ with

$$\begin{aligned}\delta = {} & 4L_X \cos\left(\left(\pi - \sqrt{3}\sigma\right)/2\right) \\ & + \left\|\mathbf{t}_B^k\right\| \begin{cases} 1 - \cos(\alpha) & \text{if } \alpha < \sqrt{3}\sigma, \\ \cos\left(\alpha - \sqrt{3}\sigma\right) - \cos(\alpha) & \text{otherwise.} \end{cases}\end{aligned} \tag{27}$$

The proof for the second plane normal $\mathbf{m}_j^k$ is similar and omitted. □

The following Lemma 5 connects all feasibility problems and outlines their usage strategy.

Lemma 5 (Relation of Problems 1, 2 and 3)**.** *Let $(\tilde{\mathtt{R}}_X, \tilde{\mathbf{t}}_X, \tilde{\mathbf{x}}_j^k)$ with $\left\|\tilde{\mathbf{t}}_X\right\| \leq L_X$ be a parameter set for which the using* (3) *extended parameter set $(\tilde{\mathtt{R}}_X, \tilde{\mathbf{t}}_A^k, \tilde{\mathbf{x}}_j^k)$ is a feasible solution to Problem 1. Then $(\tilde{\mathbf{t}}_A^k, \tilde{\mathbf{x}}_j^k)$ is a feasible solution to Problem 2, $(\tilde{\mathbf{t}}_A^k)$ a feasible solution to the cone coplanarity constraint in* (17) *and $(\tilde{\mathbf{t}}_X)$ a feasible solution to Problem 3.*

Proof. Let $(\tilde{\mathrm{R}}_X, \tilde{\mathbf{t}}_X, \tilde{\mathbf{x}}_j^k)$ with $\left\|\tilde{\mathbf{t}}_X\right\| \leq L_X$ be a parameter set for which the using (3) extended parameter set $(\tilde{\mathrm{R}}_X, \tilde{\mathbf{t}}_A^k, \tilde{\mathbf{x}}_j^k)$ is a feasible solution to Problem 1. Then the set $(\tilde{\mathbf{t}}_A^k, \tilde{\mathbf{x}}_j^k)$ is a solution to Problem 2 by Lemma 1, thus results in intersecting cones for each correspondence. Since the coplanarity constraint is a neccessary condition for the intersection of cones, the parameter set $(\tilde{\mathbf{t}}_A^k)$ is a feasible solution to the cone coplanarity constraint on $\mathbf{t}_A^k$ in (17). By design the inequalities in (18) are satisfied for all $\mathbf{t}_X$, which create a $\mathbf{t}_A^k$ feasible to (17). Thus $\tilde{\mathbf{t}}_X$ is a solution to the inequalities (18) and following from Lemma 4 also a feasible solution to Problem 3. □

Collecting the coefficients in Problem 3 results in two affine linear constraints for every correspondence j and every motion k.

$$\mathbf{a}_j^{k\mathsf{T}}\,\mathbf{t}_X - b_j^k \geq 0 \qquad \mathbf{c}_j^{k\mathsf{T}}\,\mathbf{t}_X - d_j^k \geq 0 \tag{28}$$

To evaluate the feasibility of a parameter cube during branch-and-bound the pairs of constraints for every correspondence j and every motion k are combined into a single linear feasibility program in the three unknown components of $\mathbf{t}_X$. The feasibility of this program could be determined by any available linear programming toolkit. For improved computational efficiency, the implementation presented in this work merely checks whether the intersection of all constrained half-spaces equals the empty set or not. An empty set implicates the infeasibility of Problem 3. In this case the contraposition of Lemma 5 in (10) shows the infeasibility of Problem 1. The evaluated cube can thus be discarded safely since none of the contained parameters allows a cost improvement.

3.3. Objective Function Evaluation

The objective function evaluation step of the presented branch-and-bound optimization is performed on every cube which passes the feasibility test. The goal is to evaluate the objective function (8) on parameters inside the cube and potentially improve the currently best cost estimate $\epsilon_{\min}$. Notice that even though the goal of this work is global optimization, this step does not need to be optimal. If objective function evaluation fails to reach the global optimum inside a cube, the worst case is that $\epsilon_{\min}$ can't be improved and some infeasible cubes can't be rejected yet. No optimal solution is lost.

For simplicity, only the rotation $\bar{\mathrm{R}}_X$ represented by the cube's center is evaluated. This selection improves as the parameter volume inside the cubes reduces over runtime of the algorithm. The feasibility test based on Eq. (28) returns a feasible 3D region for $\mathbf{t}_X$ plus a single sample inside this region. Based on these two parameters, the algorithm determines the camera's relative rotation R_A^k and translation $\mathbf{t}_A^k$ from Eq. (2) and (3) respectively. Triangulation then recovers the 3D positions $\mathbf{x}_j^k$ of the interest points in the scene. To minimize computational complexity the mid-point method was selected regardless of its disadvantages. The objective function (8) finally determines the resulting cost value.

3.4. Convergence

During the execution of the algorithm, the feasible cubes successively decrease in size ($\sigma \to 0$). In the limit case, their volume converges towards the single parameter at the cube center. In this case, the relaxation terms $2\varphi_{\max} \sin\left(\sigma\sqrt{3}/2\right)$ in Problem 2 and δ in the translation constraints (21) vanish. The feasibility test then accurately decides whether the cube's center parameter yields an objective function improvement or not. The infeasibility of Problem 3 extends from a sufficient to a necessary condition for cube infeasibility in the sense of Problem 1. No cube is falsely considered feasible. Thus if the typical requirements for hand-eye calibration [2] are satisfied by the executed hand motions, the proposed algorithm converges.

4. Evaluation

This section evaluates the proposed method for global optimization of hand-eye calibration. The results were obtained using a hybrid Matlab7.11 and C prototype implementation. It was executed on an Intel Core i7 CPU with 3.3 GHz running Linux.

4.1. Sensitivity to Noise Affected Interest Points

420 synthetic calibration scenarios were generated to analyze the algorithm's sensitivity to noise affected interest point correspondences. Each synthetic scenario is composed of a set of 30 uniformly distributed 3D points in front of which the virtual hand-eye rig moves. Real world image measurements are generally expected to have an accuracy within 1 pixel [9]. Since image measurements in this work are represented as unit directional vectors, feature directions were perturbed by 21 different levels of Gaussian noise in the angular domain. The tested noise standard deviations ranging from 0 to 2×10^{-3} rad correspond to deviations of 0 to 1 pixel in the image domain, given the equidistant "f-Theta" camera model in the physical setup. The termination criteria was the feasible parameter space volume reaching a value below 1×10^{-5} rad^3. The required upper bound L_X of the hand-eye translation length was set to 1.5 times the ground truth length of $\mathbf{t}_X$. The angle of the delta-rotation between the estimated and the ground truth rotation is used to measure the accuracy of the estimated orientation. The translational error is measured as the L_2 norm between estimated and ground truth translation.

Fig. 2 illustrates the rotational and translational estimation errors over the varying noise levels. Good average estimation errors of at most 3×10^{-3} rad ($\approx 0.2\,^\circ$) are achieved

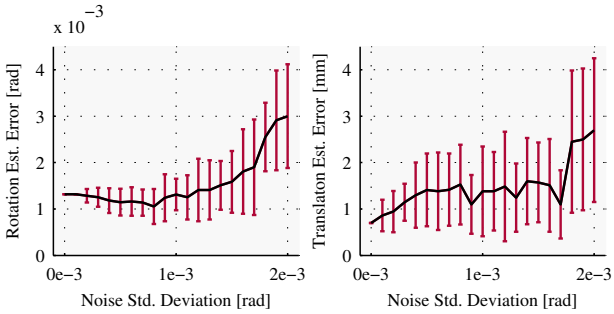

Figure 2: Rotation and translation estimation errors over increasing noise levels. The error bars show the standard deviation over the 20 experiments at each noise level.

throughout the expected noise levels. The effect of improving estimations at increasing noise levels (between 0 and 1×10^{-3} rad) was analyzed by Ruland *et al*. in [11]. The average computation time in these simulated experiments was approximately 107 s.

4.2. Benchmark Dataset

This paper introduces a benchmark dataset for hand-eye camera self-calibration in robotic vision scenarios. It is designed to provide a common point of reference for algorithm evaluation. It consists of image sequences from typical industrial scenarios including end-effector poses and additional images for intrinsic camera calibration. The benchmark dataset is included in the supplemental material in lossy compressed form and published online as original uncompressed data in full quality.

The dataset is comprised of three different scenarios. Scenario 1 (Fig 3b) is designed towards the application of reference algorithms, which rely on known calibrations objects in the scene. It mostly contains chessboard patterns in various orientations (cell size $50\text{mm} \times 50\text{mm}$). Scenario 2 features unknown objects, placed besides the calibration patterns (Fig 3c). In this scenario the results of chessboard based calibration algorithms can be verified and correspondence based algorithms observe random texture to extract image features. In scenario 3 (Fig 3d) the complete scene consists of unknown objects. The robot poses are identical throughout all three scenarios.

Fig. 3a shows the experimental camera and robot setup. A monochrome PointGrey Flea3 camera equipped with a Fujinon FE185C086HA-1 185° field of view, equidistant fish-eye lens (focal length 2.7mm) was mounted to the end-effector of a Mitsubishi RV-6S-S12 industrial robot. The camera was capturing 1280×960 pixel imagery from 25 robot poses. These robot poses positioned the end-effector on a half dome segment with the Z-axis of the end-effector frame roughly pointing towards the center of the scene.

Hand-eye reference calibrations were established in two

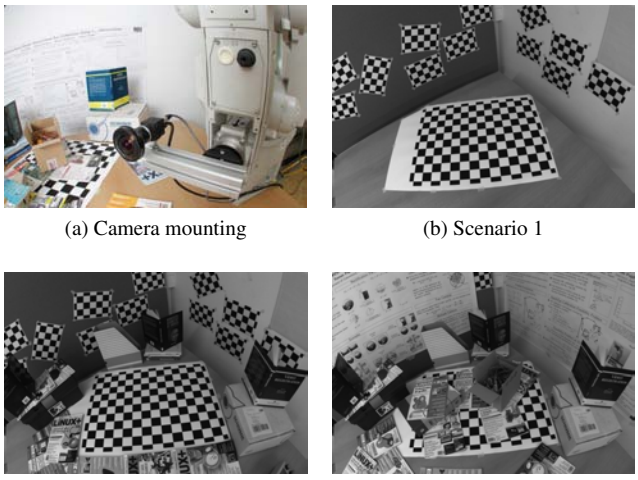

(a) Camera mounting (b) Scenario 1

(c) Scenario 2 (d) Scenario 3

Figure 3: Experimental setup and new benchmark dataset. (a) Camera mounting at the robot's end effector. (b-d) Sample images of the evaluation scenarios featuring calibration objects only, sparse and full object coverage respectively.

ways. A rough physical measurement yielded a camera position in the end-effector frame of $(40, -110, 90)^\mathsf{T}$ mm. The well known approach of Tsai and Lenz [14] was applied on pre-estimated camera poses, using the calibration patterns in scenario 1. The result was a camera position in the end-effector frame of $(44.76, -112.68, 93.75)^\mathsf{T}$ mm. The hand to camera rotation was estimated at $(0.0301, 0.1117, 0.7554)^\mathsf{T}$ rad in multiplied angle axis notation.

4.3. Evaluation on Benchmark Dataset

The evaluation was conducted using scenario 2, so that both tested and reference algorithm can be run on the same data. Of course only the reference algorithm of Tsai and Lenz [14] used the calibration patterns. From the 25 robot poses in the dataset, 100 optimization problems with two relative motions were extracted. They were selected by thresholding the angle between their rotation axes at minimum 40 °. This ensures that there is a unique solution to the hand-eye calibration problem [2]. For each motion pair 30 interest point correspondences were extracted. L_∞-approaches are generally very sensitive to outliers since they are actually fitting the noisiest data [6, 9]. Since the described method does not contain an algorithmic element of correspondence selection, outliers had to be rejected manually. The selection procedures presented in [11] fit very well into the presented optimization principle, but could not be integrated into this paper due to space constraints.

Each optimization problem was processed individually. The termination criteria was the feasible parameter space

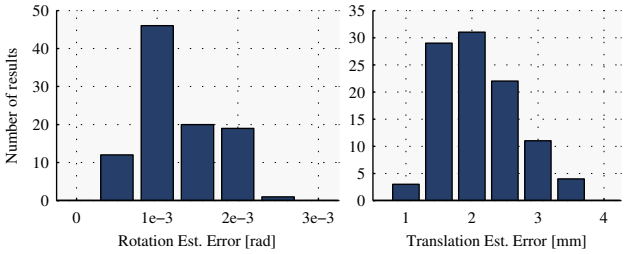

Figure 4: Evaluation results on benchmark dataset (scenario 2) after optimizing 100 problem configurations.

volume reaching a value below 1×10^{-5} rad^3. The upper bound L_X of the hand-eye translation length was set to 1.5 times the length of the manually measured $\mathbf{t}_X$. The histograms in Fig 4 visualize the algorithm's performance on the evaluation set. With average values of 2×10^{-3} rad and 2.2 mm, the achieved rotational and translational errors are in the same order of magnitude as in the simulated experiments with angular noise of standard deviation 1.7×10^{-3} rad. The average computation time of 237 s shows the low computational complexity of the presented feasibility test.

This benchmark with respect to the algorithm of Tsai and Lenz validates the algorithm's accuracy to be well suited for practical application. In contrast to the reference algorithm, the presented approach does not require known calibration objects in the scene. Hand-eye calibration can thus be performed in the natural operation environment of the robotic setup. Calibration performance is also either equal or superior to current state of the art correspondence based hand-eye calibration methods. The rotational accuracy is in the same order of magnitude or even better when compared to the results published by Seo *et al*. [13] and Ruland *et al*. [11] respectively. The translational accuracy is improved over the contribution of Heller *et al*. [7]. The unique feature of the solution presented in this work is, that both components of the hand-eye transformation are optimized simultaneously with respect to reprojection errors.

5. Conclusion

In context of the hand-eye calibration problem, gradient descent methods generally fail to reach the global optimum. Most existing hand-eye calibration solutions do not directly address reprojection errors and rely on previously estimated camera motions. Previous contributions which optimize reprojection errors, only estimate parts of the full 6 degree of freedom hand-eye transformation. This work introduced a novel method for globally optimal hand-eye self-calibration based on a geometrically meaningful objective function of reprojection errors. The design of the branch-and-bound parameter space search as a two step process enabled the main contribution of a new direct test for the feasibility of a valid hand-eye translation. The successful evaluation on both simulated and real world hand-eye calibration problems showed the algorithm to be well suited for practical applications. The public benchmark dataset creates a common point of reference for evaluation of hand-eye self-calibration algorithms and might further encourage research in this field.

Acknowledgement

The work of T. Pajdla was supported by the TACR TA 02011275 and De-Montes FP7-SME-2011 285839 grants.

References

[1] N. Andreff, R. Horaud, and B. Espiau. Robot hand-eye calibration using structure-from-motion. *Int. J. Robot. Research*, 20:228–248, 2001.

[2] H. Chen. A screw motion approach to uniqueness analysis of head-eye geometry. In *IEEE Proc. Computer Vision and Pattern Recognition*, pages 145 –151, 3-6 1991.

[3] K. Daniilidis. Hand-eye calibration using dual quaternions. *Int. J. Robot. Research*, 18:286–298, 1999.

[4] S. Esquivel, F. Woelk, and R. Koch. Calibration of a multi-camera rig from non-overlapping views. In *Pattern Recognition*, volume 4713 of *Lecture Notes in Computer Science*, pages 82–91. Springer Berlin / Heidelberg, 2007.

[5] R. I. Hartley and F. Kahl. Global optimization through rotation space search. *Int. J. Computer Vision*, 82:64–79, 2009.

[6] R. I. Hartley and F. Schaffalitzky. LX minimization in geometric reconstruction problems. In *IEEE Proc. Computer Vision and Pattern Recognition*, pages I: 504–509, 2004.

[7] J. Heller, M. Havlena, A. Sugimoto, and T. Pajdla. Structure-from-motion based hand-eye calibration using L_∞ minimization. In *IEEE Proc. Computer Vision and Pattern Recognition*, 2011.

[8] R. Horaud and F. Dornaika. Hand-eye calibration. *Int. J. Robot. Research*, 14(3):195–210, June 1995.

[9] F. Kahl and R. Hartley. Multiple-view geometry under the L_∞-norm. *IEEE Trans. Pattern Anal. Machine Intell.*, 30(9):1603 –1617, sep. 2008.

[10] F. Park and B. Martin. Robot sensor calibration: solving ax=xb on the euclidean group. *IEEE Trans. Robot. Automat.*, 10(5):717 –721, oct 1994.

[11] T. Ruland, T. Pajdla, and L. Krüger. Robust hand-eye self-calibration. In *IEEE Proc. Intell. Transport. Syst.*, 2011.

[12] J. Schmidt, F. Vogt, and H. Niemann. Calibration-free hand-eye calibration: A structure-from-motion approach. In *Pattern Recognition*, volume 3663 of *Lecture Notes in Computer Science*, pages 67–74. Springer Berlin / Heidelberg, 2005.

[13] Y. Seo, Y. J. Choi, and S. W. Lee. Branch-and-bound algorithm for globally optimal calibration of a camera-and-rotation-sensor system. In *IEEE Proc. Int. Conf. Computer Vision*, pages 1173–1178, 2009.

[14] R. Tsai and R. Lenz. A new technique for fully autonomous and efficient 3d robotics hand/eye calibration. *IEEE Trans. Robot. Automat.*, 5(3):345–358, Jun 1989.